frontiers in Energy Research

BRIEF RESEARCH REPORT
published: 13 December 2021
doi: 10.3389/fenrg.2021.807300

The Role of ZnO as a Dopant and an Intergranular Phase in the Electrical Properties of $Ca_{0.6}Sr_{0.4}TiO_3$ Ceramics

Lin Zhang[1,2], *Qian Wang*[1,2], *Jie Li*[1,2]* *and Chuanhui Wang*[1,2]

[1]School of Physics and Mechanical and Electronical Engineering, Institute for Functional Materials, Hubei University of Education, Wuhan, China, [2]Institute of Materials Research and Engineering, Hubei Engineering Technology Research Center of Environmental Purification Materials, Hubei University of Education, Wuhan, China

ZnO was introduced into $Ca_{0.6}Sr_{0.4}TiO_3$ ceramics as a dopant and an intergrangular phase in this research, followed by detailed structure characterization, energy storage performance analysis, and electrical behavior studies. The results revealed that the existence of ZnO as a dopant led to the decrease of conduction activation energy and the deterioration of energy storage behavior, while appropriate introduction of ZnO as an intergranular phase resulted in the increase of conduction activation energy and the optimization of energy storage performance. Additionally, the inverse relation between interfacial polarization and energy storage performance was observed in this study. Finally, an increased energy storage density of 1.16 J/cm^3 was achieved in 1 mol% ZnO-added $Ca_{0.6}Sr_{0.4}TiO_3$ ceramics.

Keywords: ZnO, dopants, intergranular phases, energy storage performance, interfacial polarization

OPEN ACCESS

Edited by:
Chao Han,
University of Technology Sydney, Australia

Reviewed by:
Baoyan Fan,
Chongqing University of Science and Technology, China
Pin Liu,
Nanjing Normal University, China

***Correspondence:**
Jie Li
lijie@hue.edu.cn

Specialty section:
This article was submitted to Electrochemical Energy Conversion and Storage, a section of the journal Frontiers in Energy Research

Received: *02 November 2021*
Accepted: *18 November 2021*
Published: *13 December 2021*

Citation:
Zhang L, Wang Q, Li J and Wang C (2021) The Role of ZnO as a Dopant and an Intergranular Phase in the Electrical Properties of $Ca_{0.6}Sr_{0.4}TiO_3$ Ceramics. Front. Energy Res. 9:807300. doi: 10.3389/fenrg.2021.807300

1 INTRODUCTION

Dielectric capacitors, which store and release electric energy through the reorientation of dipoles, possess ultrahigh power densities, being suitable for occasions that need a large amount of energy to be released in a short time, such as pulse power systems, which are extensively applied in hybrid electric vehicles, avionics, oil drilling, and high-power lasers for military applications (Hao, 2013; Fan et al., 2018; Li et al., 2018; Palneedi et al., 2018; Tan, 2020; Yao et al., 2020; Li et al., 2021; Wang et al., 2021). Among commercial ceramic dielectrics, $Ca_{1-x}Sr_xTiO_3$ solid solutions are considered to be promising candidates due to their high intrinsic breakdown strength (BDS), low dielectric loss, good temperature/bias voltage stability of dielectric constant. However, lower BDS in practice, which resulted from the defects (pores, secondary phases, abnormally grown grains, oxygen vacancies, etc.) produced during the high-temperature sintering process (>1,350°C) (Zhang et al., 2016; Zhang et al., 2017; Zhou et al., 2018), retarded the further development of this system. Hence, decreasing the sintering temperature, accompanied by optimizing the microstructure, is of great significance in $Ca_{1-x}Sr_xTiO_3$ ceramics.

Generally, the reduction of sintering temperature and the optimization of the microstructure are realized simultaneously, in which the approaches including the reforming of the sintering process (two-step sintering, microwave sintering, and spark plasma sintering) (Liu et al., 2017a; Liu et al., 2017b; Liu et al., 2019), the doping of selected ions (Bi^{3+}, Nd^{3+}) (Wang et al., 2018; Zhu et al., 2021), the addition of glasses (Bi_2O_3-B_2O_3-ZnO, BaO-SrO-Nb_2O_5-Al_2O_3-B_2O_3-SiO_2) (Wang et al., 2017; Song et al., 2018), and the addition of oxides (CuO, ZnO, MgO, SiO_2, and MnO_2) (Dong et al., 2009; Huang et al., 2015; Muhammad et al., 2016; Pu et al., 2017; Qu et al., 2017; Huang et al., 2018; Tao et al., 2018; Yao et al., 2018; Huang et al., 2019; Li et al., 2020). The approaches mentioned above can

usually lead to low porosity, fine grains, and uniform distribution of grain size, and thus, the spread of the conduction pathway can be delayed to the largest extent; thus, the BDS could be enhanced, and finally, the energy storage densities could be notably improved. Among the above approaches, the addition of oxides was widely adopted; for example, Qu et al. prepared $0.9(K_{0.5}Na_{0.5})NbO_3$-$0.1Bi(Mg_{2/3}Nb_{1/3})O_3$-$x$ mol%CuO (x = 0, 0.25, 0.5, 1.0, and 1.5) ceramics and found that with the increase of CuO amount, the sintering temperature was notably reduced to lower than 1,000°C, while the densification of the ceramics was increased, leading to a large BDS of 400 kV/cm and a high energy storage density of 4.02 J/cm^3 at a composition of x = 1.0 (Qu et al., 2017). Additionally, Huang et al. prepared (100-x)wt% $Ba_{0.4}Sr_{0.6}TiO_3$-$x$wt%MgO composites (x = 3, 5, 10) and found that the BDS was greatly improved with the increase of MgO amount; finally, a high BDS of 300 kV/cm and a large energy storage density of 1.50 J/cm^3 were achieved (Huang et al., 2015). However, the way oxides are introduced into ceramics will lead to different existence forms of oxides, that is, as dopants or as intergranular phases; thus, their effect mechanisms are different, and ultimately, the influence rules on the macroscopic properties are also different.

Based on this, $Ca_{0.6}Sr_{0.4}TiO_3$ (CST) was selected as the research object in this study, and ZnO was chosen to be introduced into CST, with the aim of tailoring the microstructure and the macroscopic electric properties. To be specific, ZnO will be introduced into CST as a dopant and an intergranular phase, followed by detailed structure characterization, energy storage performance analysis, and electrical behavior studies. In this research, the role of ZnO in the energy storage performance and the electric conduction behavior of CST were investigated comprehensively.

2 EXPERIMENTAL PROCEDURE

2.1 Sample Preparation

$Ca_{0.6}Sr_{0.4}TiO_3$-$x$mol%ZnO_2 (x = 0, 1, 5, 20) was fabricated *via* a solid-state reaction method. First, ZnO was introduced into $Ca_{0.6}Sr_{0.4}TiO_3$ (CST) as a dopant, marked as process route 1. In this route, $CaCO_3$, $SrCO_3$, TiO_2, and ZnO_2 powders were batched stoichiometrically and ball-milled with zirconium media in ethanol for 24 h. After drying, the powders were granulated and pressed to form disk-shaped samples with 12 mm in diameter and 1 mm in thickness. Then, the green pellets were sintered at 1,400°C for 2 h.

Second, ZnO was introduced into CST as an intergranular phase, marked as process route 2. In this route, CST powders with the perovskite phase were pre-synthesized; to be specific, $CaCO_3$, $SrCO_3$, and TiO_2 powders were mixed and ball-milled in ethanol for 24 h, and after drying, the powders were pre-calcined at 1,200°C for 2 h, followed by second calcination at 1,400°C for 3 h. Then, the porcelained powders were remilled, mixed with ZnO, and ball-milled again for 24 h. After drying, granulation, and pressing, the achieved green pellets were sintered at 1,180°C for 1 h. It needs to be noted that to prepare composites successfully, the final sintering temperature should not be too high (Pan et al., 2015; Zhang et al., 2015; Wu et al., 2016) since the high temperature not only leads to the diffusion and chemical reaction between the matrix and ZnO but also results in the decomposition of ZnO and the volatilization of Zn. Additionally, the heating rate is set to 10°C/min, with the aim of avoiding the chemical reaction between CST and ZnO.

2.2 Structure and Property Characterization

XRD analysis was performed on as-sintered and polished pellets using X-ray diffraction (XRD) (X'Pert PRO, PANalytical, Holland). The microstructure was observed on the surface of sintered samples using a scanning electron microscope (SEM) (Quanta FEG 450, FEI, USA). Impedance spectroscopy was measured using a precision impedance analyzer (E4980A, Agilent, USA) connected with an external furnace. To determine the polarization versus electric field (P-E) hysteresis loops, sintered samples were polished to 0.3 mm in thickness and measured using a ferroelectric material test system (HVI0403-239, Radiant Technology, USA) in a silicone oil bath. The charged/discharged energy density was estimated from the P-E curves by integrating the area enclosed within the polarization axis and the charged/discharged curve. The energy storage efficiency was decided by the ratio of discharged and charged energy density.

3 RESULTS AND DISCUSSION

3.1 Structure Analysis

Figure 1 compares the XRD patterns of CST-based ceramics when ZnO was introduced through process routes 1 and 2. It can be observed that when prepared *via* process route 1, only a single CST perovskite phase was revealed, indicating that ZnO was dissolved into the CST phase due to the little difference of radii for Zn^{2+} (0.74 Å) and Ti^{4+} (0.605 Å) (Li et al., 2020). However, secondary phases were observed in CST ceramics when ZnO was introduced *via* process route 2, as seen in **Figure 1B**, especially under 5 mol% and 20 mol% ZnO conditions. Additionally, the secondary phase was indexed as ZnO according to the JCPDS card.

The surface morphology of CST ceramics prepared through process routes 1 and 2 was observed *via* SEM images, as given in **Supplementary Figure S1** (route 1) and **Supplementary Figure S2** (route 2), in which a dense and pore-free microstructure was revealed. It appears that the doping amount had little influence on the average grain size (~3–4 μm) of CST ceramics when ZnO was introduced as a dopant (process route 1); at the same time, a uniform grain size distribution was observed (for simplicity, only the SEM image of 20 mol% Zn-doped CST ceramics is given, as illustrated in the insets of **Figure 1A**), which also indicates the single phase in CST ceramics, consistent with the XRD results. However, when ZnO was introduced as an intergranular phase (process route 2), the average grain size was notably reduced to ~1–1.5 μm, accompanied with a duplex distribution of very big grains (1.5–2.5 μm) and very small grains (about 0.5 μm) (for simplicity, only the SEM image of 20 mol% Zn-added CST ceramics is given, as illustrated in the insets of **Figure 1B**).

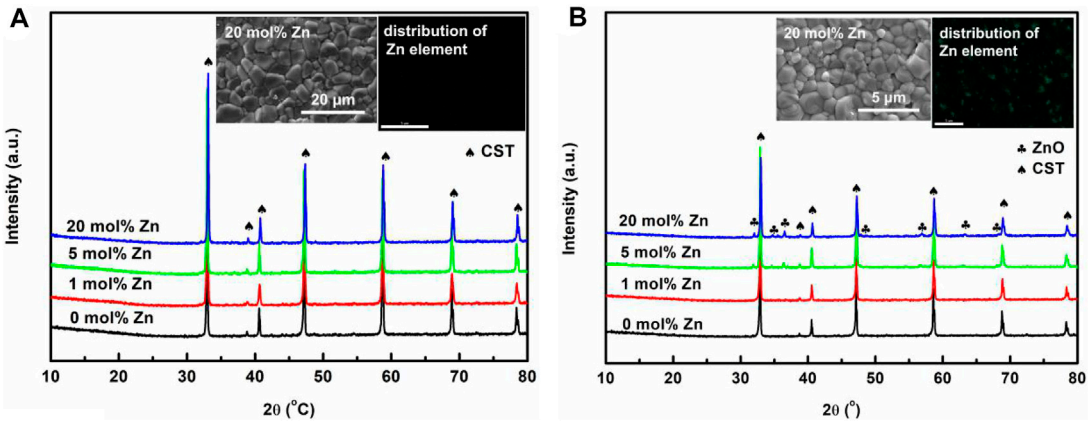

FIGURE 1 | XRD patterns for CST-ZnO ceramics prepared *via* **(A)** process route 1 and **(B)** process route 2, and the insets are the SEM images and the distribution of the Zn element for CST-20 mol% ZnO ceramics.

The notably reduced grain size was attributed to the low sintering temperature (1,180°C) and the short sintering time (1 h) of process route 2, which provided insufficient energy for the growth of grains. Additionally, the duplex distribution of big grains and small grains implies the coexistence of the CST phase and ZnO phase in the ceramic composites, consistent with the results of XRD.

The element distribution of Ti and Zn, achieved from the EDS mapping, also confirmed the coexistence of the CST phase and ZnO phase. Since uniform distribution of the Ti and Zn elements was revealed from the surface of CST-20 mol% Zn ceramics prepared *via* process route 1, as given in the insets of **Figure 1A**, on the contrary, a non-uniform distribution of the Ti and Zn elements was observed in CST-20 mol% Zn ceramics when prepared through process route 2, as seen in the insets of **Figure 1B**.

Thus, structure analysis, including XRD and SEM, indicates that ZnO was introduced as a dopant in process route 1; however, when *via* process route 2, ZnO was introduced as an intergranular phase successfully, no obvious chemical diffusion and reaction was revealed, consistent with our research expectation.

3.2 Energy Storage Performance

The energy storage properties were measured from 25 to 150°C for CST-ZnO ceramics since the CST matrix has shown potential applications at high temperature in a previous research study (Zhang et al., 2017). The P-E loops measured at room temperature and the critical electric field for CST-ZnO ceramics prepared *via* process routes 1 and 2 are given in **Supplementary Figure S3** (route 1) and **Supplementary Figure S4** (route 2), in which the BDS, the recoverable energy storage density (W), and the energy storage efficiency (η) are calculated and listed, and some interesting phenomena are revealed.

To be specific, the energy storage performance for CST ceramics was obviously deteriorated when ZnO was introduced *via* process route 1, where the BDS decreased from 26 kV/mm of pure CST to 20 kV/mm of 20 mol% ZnO-doped CST, and at the same time, the recoverable energy storage density was reduced from 0.964 J/cm^3 to 0.483 J/cm^3. Thus, the doping of ZnO contributes to the energy storage performance of CST ceramics as a negative factor.

However, the energy storage properties for CST ceramics experienced a significant increase at first and then a slight decrease with the increase of ZnO amount, when they were introduced *via* process route 2. It can be observed from **Supplementary Figure S4** that the BDS increased from 16 kV/mm of pure CST to 28 kV/mm of 1 mol% ZnO-added CST, and at the same time, the recoverable energy storage density was increased from 0.347 J/cm^3 to 1.164 J/cm^3. Hence, the introduction of a moderate amount of ZnO as an intergranular phase is beneficial for the enhancement of the energy storage performance for CST ceramics.

The P-E loops illustrated in **Figure 2** were measured at a high temperature (150°C), in which the same evolution trend with room temperature was revealed; that is, the energy storage performance was deteriorated when ZnO was introduced as a dopant, while significant improvement of the energy storage behavior was observed when moderate ZnO was introduced as an intergranular phase. Consequently, not only the amount but also the way ZnO was introduced into CST has a significant effect on energy storage performance. Based on this, the influence rules on the macroscopic properties and the effect mechanisms of ZnO should be investigated and unveiled cautiously.

3.3 Electrical Behavior Study

The AC conductivities for CST-ZnO ceramics were measured and analyzed over the temperature range of 400–500°C and the frequency range of 20 Hz to 2 MHz, as shown in **Figure 3A**. The conductivity peaks were found to shift to a higher frequency with ascending temperature, indicating notable thermal-activated dielectric relaxation. The dielectric relaxation occurring at 400–500 °C was considered to be induced by the migration of oxygen vacancies (Zhang et al., 2018), which are considered as the main contributor to the ionic conductivity in polycrystalline ceramics. Additionally, the conduction activation energies of CST-ZnO ceramics can be calculated by Arrhenius fitting as

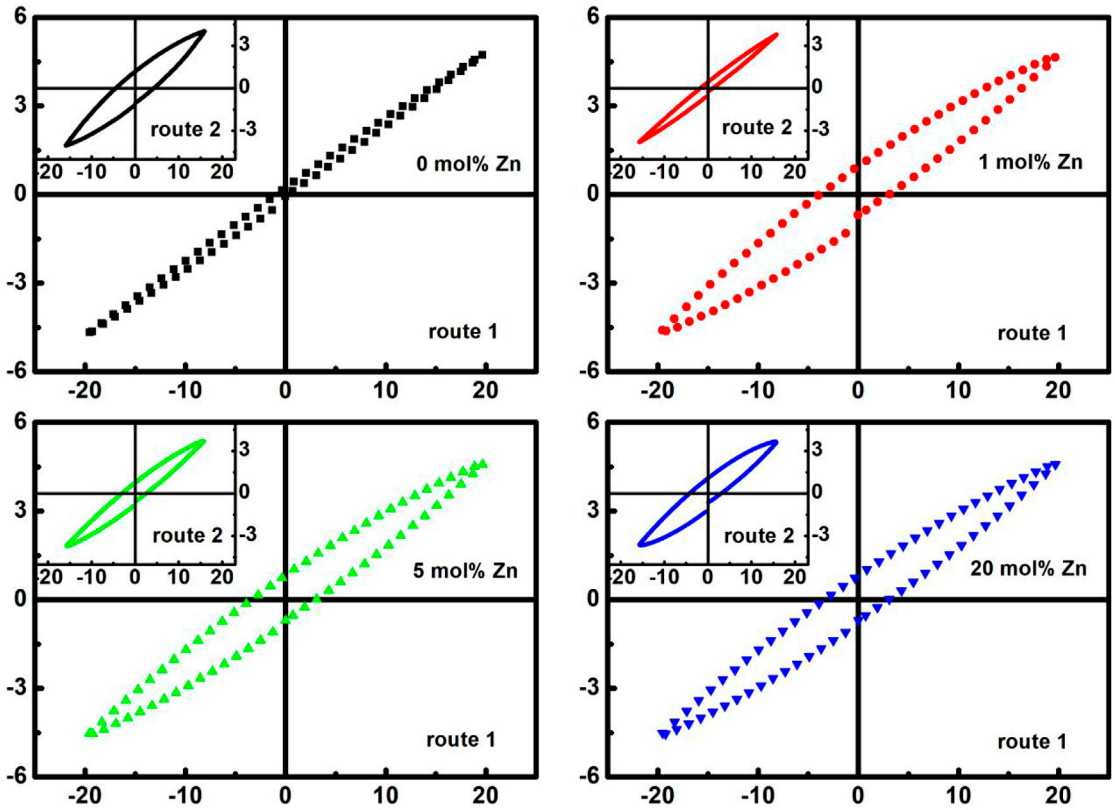

FIGURE 2 | P-E loops measured at 150°C and 20 kV/mm for CST-ZnO ceramics prepared *via* process route 1; the insets show P-E loops measured at 150°C and 16 kV/mm for CST-ZnO ceramics prepared *via* process route 2.

$$\sigma_{dc} = \sigma_0 \exp\left(-\frac{E_a}{k_B T}\right),$$

where σ_{dc} is the DC conductivity, σ_0 the pre-exponential factor, E_a is the conduction activation energy, and k_B is the Boltzmann constant. Conductivities at 20 Hz in this case were taken as DC conductivities because the conductivities almost remain constant in the low-frequency range.

The fitting results of the activation energies for CST-ZnO ceramics are listed in **Supplementary Figure S5** (route 1), **Supplementary Figure S6** (route 2), and **Table 1**, where the completely different evolution trend with increasing ZnO amount between process routes 1 and 2 was revealed. When ZnO was introduced *via* route 1 and as a dopant, the conduction activation energies directly decreased with increasing doping amount, indicating that the migration of oxygen vacancies is getting easier; thus, the ionic conductivity increased, accompanying with the deterioration of the energy storage performance. However, when ZnO was introduced *via* route 2 and as an intergranular phase, the conduction activation energies significantly increased first and then experienced a slight decrease, indicating that introducing moderate ZnO can retard the migration of oxygen vacancies, and consequently resulted in notably improved energy storage behavior.

Additionally, to investigate the effect of ZnO on grain and grain boundary regions of CST ceramics, complex impedance spectra were recorded since useful information can be revealed by this method for polycrystalline ceramics demonstrating a heterogeneous electrical structure, as shown in **Figures 3B,C**. The typical two semicircular arcs in the impedance spectra are closely related to the response of grain (conductive and appears at a high frequency) and grain boundary (resistive and appears at a low frequency) regions (Guo and Maier, 2001; Harrington and Devine, 2009). More importantly, the resistance of grain and grain boundary regions can be achieved through Z-view software fitting with the 2RQ equivalent circuit model, as explained in detail in a previous study (Zhang et al., 2016), and the fitting results are given in **Table 1**.

It can be observed from **Figures 3B,C** that not only the grain boundary but also the grain region was affected by the introduction of ZnO. When ZnO was introduced *via* process route 1 and as a dopant, both the insulating properties of grains and grain boundaries were deteriorated due to the increased concentration of oxygen vacancies caused by the doping of Zn^{2+} at the Ti^{4+} site, that is, $ZnO \xrightarrow{TiO_2} Zn''_{Ti} + O_O + V_o^{\bullet\bullet}$. However, when ZnO was introduced through process route 2 and as an intergranular phase, the evolution trend is totally different, where both the insulating properties of grains and grain boundaries were improved, especially under 1 mol% Zn conditions. As it is widely known that ZnO is an oxide with high insulating nature, which can be more resistive than CST grains, the existence of ZnO

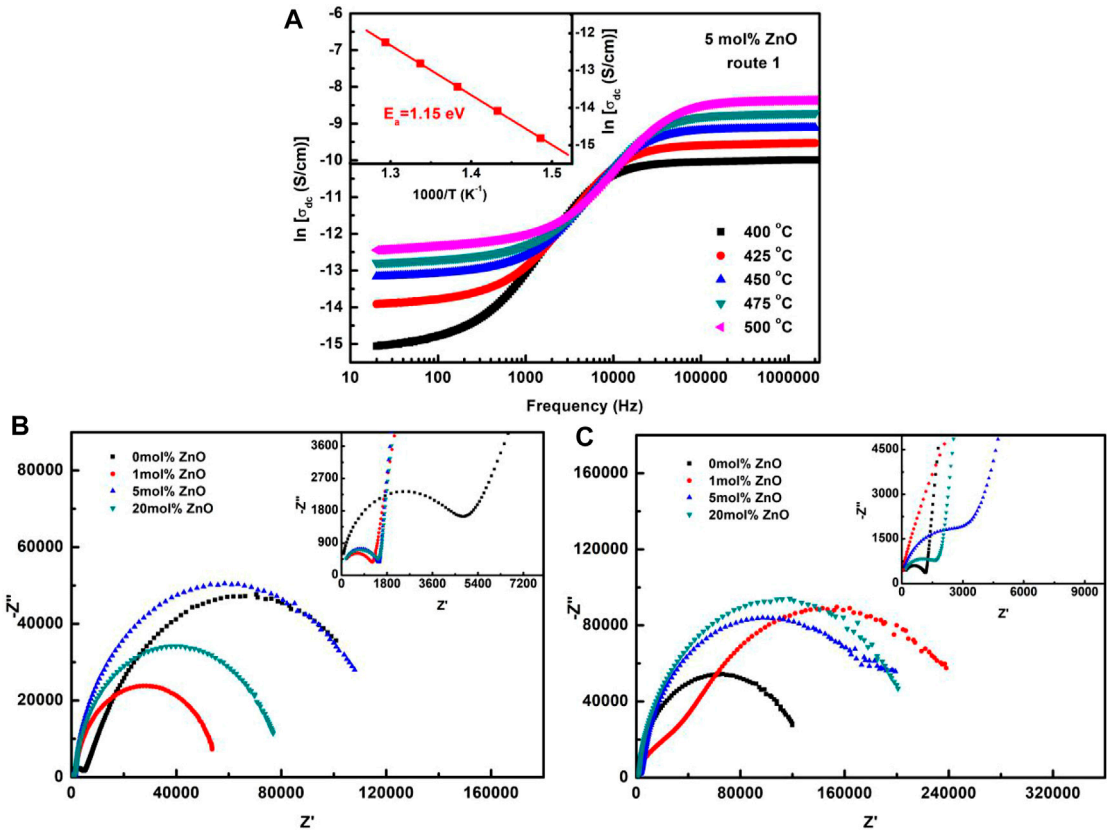

FIGURE 3 | (A) AC conductivity and Arrhenius fitting results for CST-5mol% ZnO ceramics prepared *via* process route 1 and complex impedance spectra (at 425°C) for CST-ZnO ceramics prepared *via* **(B)** process route 1 and **(C)** process route 2.

TABLE 1 | BDS and fitting results of R_{gb}, R_g, and E_a for CST-ZnO ceramics prepared *via* process routes 1 and 2

	(%)	R_{gb} (Ω)	R_g(Ω)	R_{gb}/R_g	E_a (eV)	BDS@RT (kV/mm)	W_{rec}@RT (J/cm^3)	η@RT (%)
Process route 1	0 mol	134,690	4,905	27	1.62	26	0.964	90
	1 mol	54,654	1,279	43	1.41	22	0.656	97
	5 mol	113,090	1,487	76	1.15	20	0.549	96
	20 mol	76,446	1,513	51	1.21	20	0.483	93
Process route 2	0 mol	124,250	1,183	105	1.19	16	0.347	82
	1 mol	253,400	24,911	10	1.41	28	1.164	93
	5 mol	205,910	3,741	55	1.27	26	0.862	91
	20 mol	213,270	1870	114	1.02	22	0.581	90

@RT means at room temperature.

as an intergranular phase will be beneficial for the charge transportation between grain and grain boundary regions, promoting the diffusion of local charge, suppressing the degree of interfacial polarization, and finally resulting in improved BDS and energy storage densities.

Additionally, interfacial polarization in this study can be quantified by the values of R_{gb}/R_g, as given in **Table 1**. It is obvious that when ZnO was introduced as a dopant, the interfacial polarization was promoted, the conduction activation energies were decreased, and the BDS was decreased too. On the contrary, the appropriate introduction of ZnO as an intergranular phase led to depressed interfacial polarization, increased conduction activation energies, and improved BDS of CST ceramics. It is worth noting that excess introduction of ZnO will lead to the non-uniform distribution of the intergranular phase in the CST matrix, which is not beneficial

for charge diffusion and the optimization of BDS and energy storage densities.

4 CONCLUSION

ZnO was selected to be introduced into CST ceramics as a dopant and an intergranular phase in this study to modify the energy storage behavior. The introduction of ZnO as a dopant resulted in decreased conduction activation energies, promoted interfacial polarization, and deteriorated energy storage performance. However, suitable introduction of ZnO as an intergranular phase led to increased conduction activation energies, depressed interfacial polarization, and enhanced energy storage properties. Thus, the energy storage behavior of CST ceramics is sensitive not only to the amount of ZnO but also to its existence form.

DATA AVAILABILITY STATEMENT

The raw data supporting the conclusion of this article will be made available by the authors, without undue reservation.

AUTHOR CONTRIBUTIONS

LZ is responsible for the collation of data and the writing of the manuscript; QW is responsible for the fitting of data; JL is responsible for the construction of the manuscript framework and the revision of the manuscript; CHW is responsible for the drawing of graphs.

FUNDING

This work was supported by the Natural Science Foundation of Hubei Province of China (No. 2020CFB245) and the Science and Technology Research Program of the Education Department from Hubei Province of China (Nos. Q20193002 and B2021260).

SUPPLEMENTARY MATERIAL

The Supplementary Material for this article can be found online at: https://www.frontiersin.org/articles/10.3389/fenrg.2021.807300/full#supplementary-material

REFERENCES

Dong, G., Ma, S., Du, J., and Cui, J. (2009). Dielectric Properties and Energy Storage Density in ZnO-Doped Ba0.3Sr0.7TiO3 Ceramics. *Ceramics Int.* 35 (5), 2069–2075. doi:10.1016/j.ceramint.2008.11.003

Fan, B., Liu, F., Yang, G., Li, H., Zhang, G., Jiang, S., et al. (2018). Dielectric Materials for High-temperature Capacitors. *Iet Nanodielectrics* 1 (1), 32–40. doi:10.1049/iet-nde.2018.0002

Guo, X., and Maier, J. (2001). Grain Boundary Blocking Effect in Zirconia: A Schottky Barrier Analysis. *J. Electrochem. Soc.* 148 (3), E121–E126. doi:10.1149/1.1348267

Hao, X. H. (2013). A Review on the Dielectric Materials for High Energy-Storage Application [J]. *J. Adv. Dielectrics* 3 (1), 1330001. doi:10.1142/s2010135x13300016

Harrington, S. P., and Devine, T. M. (2009). Relation between the Semiconducting Properties of a Passive Film and Reduction Reaction Rates. *J. Electrochem. Soc.* 156 (4), C154–C159. doi:10.1149/1.3077576

Huang, Y. H., Liu, B., and Liu, X. Q. (2019). Defect Dipoles Induced High-Energy Storage Density in Mn-Doped BST Ceramics Prepared by Spark Plasma Sintering [J]. *J. Am. Ceram. Soc.* 102 (4), 1904–1911.

Huang, Y. H., Wu, Y. J., Liu, B., Yang, T. N., Wang, J. J., Li, J., et al. (2018). From Core-Shell Ba0.4Sr0.6TiO3@SiO2 Particles to Dense Ceramics with High Energy Storage Performance by Spark Plasma Sintering. *J. Mater. Chem. A.* 6, 4477–4484. doi:10.1039/c7ta10821d

Huang, Y. H., Wu, Y. J., Qiu, W. J., Li, J., and Chen, X. M. (2015). Enhanced Energy Storage Density of Ba 0.4 Sr 0.6 TiO 3 -MgO Composite Prepared by Spark Plasma Sintering. *J. Eur. Ceram. Soc.* 35 (5), 1469–1476. doi:10.1016/j.jeurceramsoc.2014.11.022

Li, D., Zeng, X., Li, Z., Shen, Z.-Y., Hao, H., Luo, W., et al. (2021). Progress and Perspectives in Dielectric Energy Storage Ceramics. *J. Adv. Ceram.* 10 (4), 675–703. doi:10.1007/s40145-021-0500-3

Li, Q., Yao, F.-Z., Liu, Y., Zhang, G., Wang, H., and Wang, Q. (2018). High-Temperature Dielectric Materials for Electrical Energy Storage. *Annu. Rev. Mater. Res.* 48 (1), 219–243. doi:10.1146/annurev-matsci-070317-124435

Li, Y., Zhang, L., Yu, L., Li, D., Meng, H., Ai, Q., et al. (2020). Study of the Structure, Electrical Properties, and Energy Storage Performance of ZnO-Modified Ba0.65Sr0.245Bi0.07TiO3 Pb-free Ceramics. *Ceramics Int.* 46 (1), 8–16. doi:10.1016/j.ceramint.2019.08.111

Liu, B., Wang, X., Zhang, R., and Li, L. (2017). Energy Storage Properties of Ultra fine-grained Ba0.4Sr0.6TiO3-Based Ceramics Sintered at Low Temperature. *J. Alloys Comp.* 691, 619–623. doi:10.1016/j.jallcom.2016.08.317

Liu, B., Wang, X., Zhang, R., and Li, L. (2017). Grain Size Effect and Microstructure Influence on the Energy Storage Properties of fine-grained BaTiO3 -based Ceramics. *J. Am. Ceram. Soc.* 100 (8), 3599–3607. doi:10.1111/jace.14802

Liu, B., Wu, Y., Huang, Y. H., Song, K. X., and Wu, Y. J. (2019). Enhanced Dielectric Strength and Energy Storage Density in BaTi0.7Zr0.3O3 Ceramics via Spark Plasma Sintering. *J. Mater. Sci.* 54 (6), 4511–4517. doi:10.1007/s10853-018-3170-y

Muhammad, Q. K., Waqar, M., Rafiq, M. A., Rafiq, M. N., Usman, M., and Anwar, M. S. (2016). Structural, Dielectric, and Impedance Study of ZnO-Doped Barium Zirconium Titanate (BZT) Ceramics. *J. Mater. Sci.* 51, 10048–10058. doi:10.1007/s10853-016-0231-y

Palneedi, H., Peddigari, M., Hwang, G.-T., Jeong, D.-Y., and Ryu, J. (2018). High-Performance Dielectric Ceramic Films for Energy Storage Capacitors: Progress and Outlook. *Adv. Funct. Mater.* 28 (42), 1803665. doi:10.1002/adfm.201803665

Pan, Z., Chen, J., Fan, L., Zhang, J., Zhang, S., Huang, Y., et al. (2015). Enhanced Piezoelectric Properties and Thermal Stability in the (K0.5 Na0.5)NbO3 :ZnO Lead-Free Piezoelectric Composites. *J. Am. Ceram. Soc.* 98 (12), 3935–3941. doi:10.1111/jace.13831

Pu, Y., Yao, M., Zhang, L., and Chen, M. (2017). Enhanced Energy Storage Density of 0.55Bi0.5Na0.5TiO3-0.45Ba0.85Ca0.15Ti0.85Zr0.1Sn0.05O3 with MgO Addition. *J. Alloys Comp.* 702, 171–177. doi:10.1016/j.jallcom.2017.01.249

Qu, B., Du, H., Yang, Z., and Liu, Q. (2017). Large Recoverable Energy Storage Density and Low Sintering Temperature in Potassium-Sodium Niobate-Based Ceramics for Multilayer Pulsed Power Capacitors. *J. Am. Ceram. Soc.* 100 (4), 1517–1526. doi:10.1111/jace.14728

Song, J., Han, L., Liu, T., Feng, Q., Luo, Z., and Lu, A. (2018). Microstructures and Energy Storage Properties of BSN Ceramics with Crystallizable Glass Addition. *J. Mater. Sci. Mater. Electron.* 29 (7), 5934–5943. doi:10.1007/s10854-018-8566-6

Tan, D. Q. (2020). Review of Polymer-Based Nanodielectric Exploration and Film Scale-Up for Advanced Capacitors. *Adv. Funct. Mater.* 30 (18), 1808567. doi:10.1002/adfm.201808567

Tao, C.-W., Geng, X.-Y., Zhang, J., Wang, R.-X., Gu, Z.-B., and Zhang, S.-T. (2018). Bi0.5Na0.5TiO3-BaTiO3-K0.5Na0.5NbO3:ZnO Relaxor Ferroelectric Composites with High Breakdown Electric Field and Large Energy Storage

Properties. *J. Eur. Ceram. Soc.* 38 (15), 4946–4952. doi:10.1016/j.jeurceramsoc.2018.07.006

Wang, D., Fan, Z., Zhou, D., Khesro, A., Murakami, S., Feteira, A., et al. (2018). Bismuth Ferrite-Based lead-free Ceramics and Multilayers with High Recoverable Energy Density. *J. Mater. Chem. A.* 6 (9), 4133–4144. doi:10.1039/c7ta09857j

Wang, G., Lu, Z., Li, Y., Li, L., Ji, H., Feteira, A., et al. (2021). Electroceramics for High-Energy Density Capacitors: Current Status and Future Perspectives. *Chem. Rev.* 121 (10), 6124–6172. doi:10.1021/acs.chemrev.0c01264

Wang, Y., Pu, Y., Cui, Y., Shi, Y., and Zheng, H. (2017). Enhanced Energy Storage Density of Ba 0.4 Sr 0.6 TiO 3 Ceramics with Additive of Bi 2 O 3 -B 2 O 3 -ZnO Glass. *Mater. Lett.* 201, 203–206. doi:10.1016/j.matlet.2017.05.007

Wu, G.-J., Nie, P.-X., Zhang, J., Cui, Y.-S., and Zhang, S.-T. (2016). Composition and Temperature Dependent Electrical Properties of BaTiO 3 :ZnO Composites. *Mater. Lett.* 164, 303–307. doi:10.1016/j.matlet.2015.11.009

Yao, F.-Z., Yuan, Q., Wang, Q., and Wang, H. (2020). Multiscale Structural Engineering of Dielectric Ceramics for Energy Storage Applications: from Bulk to Thin Films. *Nanoscale* 12 (33), 17165–17184. doi:10.1039/d0nr04479b

Yao, Y., Li, Y., Sun, N., Du, J., Li, X., Zhang, L., et al. (2018). Enhanced Dielectric and Energy-Storage Properties in ZnO-Doped 0.9(0.94Na0.5Bi0.5TiO3–0.06BaTiO3)–0.1NaNbO3 Ceramics. *Ceramics Int.* 44 (6), 5961–5966. doi:10.1016/j.ceramint.2017.12.174

Zhang, J., Pan, Z., Guo, F.-F., Liu, W.-C., Ning, H., Chen, Y. B., et al. (2015). Semiconductor/relaxor 0-3 Type Composites without thermal Depolarization in Bi0.5Na0.5TiO3-Based lead-free Piezoceramics. *Nat. Commun.* 6, 6615. doi:10.1038/ncomms7615

Zhang, L., Hao, H., Liu, H., Song, Z., Yao, Z., Xie, J., et al. (2016). Effect of HfO 2 Addition as Intergranular Grains on the Energy Storage Behavior of Ca 0.6 Sr 0.4 TiO 3 Ceramics. *J. Eur. Ceram. Soc.* 36 (13), 3157–3163. doi:10.1016/j.jeurceramsoc.2016.05.002

Zhang, L., Hao, H., Zhang, S., Lanagan, M. T., Yao, Z., Xu, Q., et al. (2017). Defect Structure-Electrical Property Relationship in Mn-Doped Calcium Strontium Titanate Dielectric Ceramics. *J. Am. Ceram. Soc.* 100 (10), 4638–4648. doi:10.1111/jace.14994

Zhang, L., Yao, Z., Lanagan, M. T., Hao, H., Xie, J., Xu, Q., et al. (2018). Effect of Oxygen Treatment on Structure and Electrical Properties of Mn-Doped Ca 0.6 Sr 0.4 TiO 3 Ceramics. *J. Eur. Ceram. Soc.* 38 (6), 2534–2540. doi:10.1016/j.jeurceramsoc.2018.01.027

Zhou, H. Y., Liu, X. Q., Zhu, X. L., and Chen, X. M. (2018). CaTiO3 Linear Dielectric Ceramics with Greatly Enhanced Dielectric Strength and Energy Storage Density. *J. Am. Ceram. Soc.* 101 (5), 1999–2008. doi:10.1111/jace.15371

Zhu, X., Shi, P., Kang, R., Li, S., Wang, Z., Qiao, W., et al. (2021). Enhanced Energy Storage Density of Sr0.7BixTiO3 lead-free Relaxor Ceramics via A-Site Defect and Grain Size Tuning. *Chem. Eng. J.* 420 (44), 129808. doi:10.1016/j.cej.2021.129808

Conflict of Interest: The authors declare that the research was conducted in the absence of any commercial or financial relationships that could be construed as a potential conflict of interest.

Publisher's Note: All claims expressed in this article are solely those of the authors and do not necessarily represent those of their affiliated organizations or those of the publisher, the editors, and the reviewers. Any product that may be evaluated in this article or claim that may be made by its manufacturer is not guaranteed or endorsed by the publisher.